AIAA JOURNAL
Vol. 31, No. 7, July 1993

Aeroelastic Response, Loads, and Stability of a Composite Rotor in Forward Flight

Edward C. Smith* and Inderjit Chopra†
University of Maryland, College Park, Maryland 20742

The aeroelastic response, blade and hub loads, and shaft-fixed aeroelastic stability are investigated for a helicopter with elastically tailored composite rotor blades. A new finite element-based structural analysis including nonclassical effects such as transverse shear, torsion related warping, and in-plane elasticity is integrated with the University of Maryland Advanced Rotorcraft Code (UMARC). The structural dynamics analysis is correlated against both experimental data and detailed finite element results. Correlation of rotating natural frequencies of coupled composite box-beams is generally within 5–10%. The analysis is applied to a soft-in-plane hingeless rotor helicopter in free flight propulsive trim. Changes in blade loads are relatively small; however, aeroelastic stability can be significantly improved by the use of elastic pitch-lag coupling. For example, lag mode damping can be increased 300% over a range of thrust conditions and forward speeds. The influence of attached flow unsteady aerodynamics on the blade response and vibratory hub loads is also investigated. The magnitude and phase of the flap response is substantially altered by the unsteady aerodynamic effects. Vibratory hub loads increase up to 30% due to unsteady aerodynamic effects.

Introduction

RESEARCH on elastically tailored composite rotor blades has increased steadily during the past decade. Pioneering studies by Hong and Chopra[1,2] and Panda and Chopra[3] indicated potential for improved aeroelastic stability and reduced vibration using elastically coupled composite rotor blades. The potential for elastically tailored, coupled structures to improve the performance of tilt-rotor vehicles was demonstrated by Nixon.[4] Since these initial studies, much of the work on composite rotors has been directed toward predicting the cross-section properties of composite beam structures and gaining a fundamental understanding of elastically coupled structures. Cross-section and static deflection analyses have been carried out using both finite element methods[5–15] and direct analytical methods.[16–25] Using both of these tools, the level of understanding about coupled composite beams has increased considerably. It has become apparent that nonclassical effects, such as transverse shear (especially bending-shear couplings) and warping, play a significant role in the static behavior of coupled composite beams.[18,24,25] For example, transverse shear-related couplings can dramatically increase the compliance of extension-torsion coupled beams under bending loads.

The dynamic behavior of composite beams has also been the focus of much research. Free vibration of nonrotating composite beams was studied by several researchers.[26–33] Many of these studies were for solid section or plate-like beams. For thin-walled composite beams, the importance of nonclassical effects was also observed in the free vibration results.[33] There have also been investigations on the structural dynamics of rotating composite beams and rotor blades.[12,15,34,35] In Ref. 15, a detailed cross-section finite element model was combined with a spanwise finite element model to predict the nonrotating and rotating frequencies and mode shapes of composite beams and advanced composite turbopropellers. These studies included detailed cross-section modeling; however, transverse shear effects were not considered. An experimental and analytical study on the rotating and nonrotating frequencies and mode shapes of coupled composite box-beams was recently conducted.[34] In this study, experimental results obtained by vacuum chamber testing were compared to a Galerkin solution based on the force deformation relations provided in Ref. 24. This study, which included the effects of transverse shear couplings (but neglecting direct transverse shear deflections), indicated that centrifugal stiffening under rotation can decrease the effects of shear-related couplings. A similar study based on the analysis of Ref. 25 was performed for composite I-beams under rotation.[35] It further illustrated the importance of nonclassical effects such as warping restraint and shear couplings.

Very little work has been done addressing the impact of composite rotors on rotorcraft system performance. Hong and Chopra[1,2] used a simple composite beam analysis combined with a spanwise finite element discretization of the rotor blade to examine the effects of elastic coupling on the aeroelastic stability of hingeless and bearingless composite rotors in hover. The beam model (and corresponding finite element) used in this study did not include transverse shear deformation and used a simplified model of warping and in-plane ply elasticity. Despite the simple composite model, this work demonstrated the potential for elastically tailored composite rotors. Panda and Chopra[3] extended this work by examining the dynamics of composite rotors in forward flight. This work showed the potential for reduction in vibration levels using composite rotors. Recently, Rand[36] investigated the steady linear periodic response of thin-walled composite helicopter blades in forward flight ($\mu = 0.2$). A more detailed model of cross-section warping was used (compared to Refs. 1–3) in this analysis. Aerodynamic loads were determined using a frequency domain formulation of thin airfoil theory. A Galerkin approach, in conjunction with the harmonic balance method, was used to determine the steady response solution. The trim criterion was the vanishing of the first harmonic of the tip flap response. Variations in response, lift distribution, and blade section stresses were demonstrated for blades with extension-torsion and bending torsion (pitch-flap) couplings. Additional discussions addressing composite rotor blade modeling can be found in several recent review papers.[37–39]

In the present study, the aeroelastic response and vibratory blade and hub loads of a helicopter with elastically tailored

Presented as Paper 92-2566 at the AIAA/ASME/ASCE/AHS/ASC 33rd Structures, Structural Dynamics, and Materials Conference, Dallas, TX, April 13–15, 1992; received July 31, 1992; revision received Jan. 15, 1993; accepted for publication Jan. 15, 1993

*Minta Martin Fellow, Department of Aerospace Engineering, Center for Rotorcraft Education and Research; currently Assistant Professor, Aerospace Engineering Department, Pennsylvania State University, University Park, PA 16802. Member AIAA.

†Professor, Department of Aerospace Engineering, Center for Rotorcraft Education and Research. Fellow AIAA.

composite rotor blades is analyzed. The shaft-fixed aeroelastic stability is also investigated. The new analysis builds on the earlier works of Hong and Chopra[1,2] and Panda and Chopra.[3] The structural model of the blade spar, idealized as a rectangular box-beam, is modeled using an improved analysis that includes the effects of transverse shear deformation and two-dimensional in-plane elasticity. A more accurate representation of torsion-related out-of-plane warping is also included. The cross-sectional analysis has been thoroughly validated against static test data.[24] In addition to using a more refined composite spar model, the new structural model is also formulated in terms of different kinematic variables. Transverse shear degrees of freedom are now included in the beam finite element used for the rotor blade. The axial elastic deflection u_e now replaces the total axial deflection u as a kinematic variable in the energy variational. This approach, similar to that discussed in Ref. 40, improves the accuracy of the normal mode solution of the nonlinear equations of motion. The effects of attached flow unsteady aerodynamics are also studied in the present work using a time domain unsteady aerodynamic model developed by Leishman and Beddoes.[41-44] Finally, the sophistication and accuracy of aeroelastic trim analysis has been significantly increased (compared to Ref. 3). Steady rotor forces and moments are now used to update the vehicle equilibrium equations at each step of the iterative trim solution. This fully coupled trim solution simultaneously yields the nonlinear blade response, pilot controls (main rotor collective and cyclic pitch and tail rotor collective pitch), and vehicle attitude (longitudinal and lateral shaft tilt angles).

Formulation

Formulation of Hamilton's Principle

A spatial finite element beam model, based on Hamilton's principle, is formulated for composite blades undergoing extension u_e, flap and lag bending v_b and w_b, elastic torsion ϕ, and transverse shearing deformations v_s and w_s. Nonlinear equations governing the moderate deflection of the composite blades are derived. The primary structural member of the blade, i.e., the spar, is idealized as a laminated composite thin-walled box-beam. Considering the beam to be undergoing small strains and moderate deflections, the strain-displacement relations are given by

$$\epsilon_{xx} = u_e' - \lambda_T\phi'' + (\eta^2+\zeta^2)\left[\theta_0'\phi' + (\phi'^2/2)\right] - v_b''\left[\eta\cos(\theta_0+\hat{\phi}) - \zeta\sin(\theta_0+\hat{\phi})\right] - w_b''\left[\eta\sin(\theta_0+\hat{\phi}) + \zeta\cos(\theta_0+\hat{\phi})\right] \tag{1a}$$

$$\epsilon_{x\eta} = -\left(\zeta + \frac{\partial\lambda_T}{\partial\eta}\right)\phi' + v_s'\cos(\theta_0+\hat{\phi}) + w_s'\sin(\theta_0+\hat{\phi}) \tag{1b}$$

$$\epsilon_{x\zeta} = \left(\eta - \frac{\partial\lambda_T}{\partial\zeta}\right)\phi' + w_s'\cos(\theta_0+\hat{\phi}) - v_s'\sin(\theta_0+\hat{\phi}) \tag{1c}$$

where $\epsilon_{x\zeta}=0$ in the horizontal spar walls and $\epsilon_{x\eta}=0$ in the vertical spar walls. In Eqs. (1), the torsion-related out-of-plane warping function is denoted by λ_T. For a composite box-beam section, an analytical expression for the warping function is derived in Ref. 24. The rigid pitch angle θ_0 is given by the expression

$$\theta_0 = \theta_{75} + \theta_{tw}\left[(x/R) - 0.75\right] + \theta_{1c}\cos\psi + \theta_{1s}\sin\psi \tag{2}$$

and the total elastic twist $\hat{\phi}$ is given by

$$\hat{\phi} = \phi - \int_0^x w_b'v_b''\,dx \tag{3}$$

Within the anisotropic laminated plies of the spar walls, the stress-strain relations are given by

Horizontal walls:

$$\begin{Bmatrix}\sigma_{xx}\\ \sigma_{x\eta}\end{Bmatrix} = \begin{bmatrix}\bar{Q}_{11} & \bar{Q}_{16}\\ \bar{Q}_{16} & \bar{Q}_{66}\end{bmatrix}\begin{Bmatrix}\epsilon_{xx}\\ \epsilon_{x\eta}\end{Bmatrix} \tag{4}$$

Vertical walls:

$$\begin{Bmatrix}\sigma_{xx}\\ \sigma_{x\zeta}\end{Bmatrix} = \begin{bmatrix}\bar{Q}_{11} & \bar{Q}_{16}\\ \bar{Q}_{16} & \bar{Q}_{66}\end{bmatrix}\begin{Bmatrix}\epsilon_{xx}\\ \epsilon_{x\zeta}\end{Bmatrix} \tag{5}$$

In Eqs. (4) and (5), $\bar{Q}_{11}$, $\bar{Q}_{66}$, and $\bar{Q}_{16}$ are elastic constants for the composite plies. These constants are functions of ply orientation angle, ply longitudinal and transverse moduli, and ply Poisson's ratios (see Ref. 24). A more detailed modeling of two-dimensional in-plane elasticity is used to modify the preceding relations as described in Ref. 24. The variation of strain energy of the composite blade δU can be written as

$$\delta U = \int_0^R\iint_A (\sigma_{xx}\delta\epsilon_{xx} + \sigma_{x\eta}\delta\epsilon_{x\eta} + \sigma_{x\zeta}\delta\epsilon_{x\zeta})\,d\eta\,d\zeta\,dx \tag{6}$$

Substitution of the strain displacement and stress-strain equations into the expression for strain energy results in the desired variational form of the strain energy. An ordering scheme is used to systematically eliminate higher order nonlinear terms from the energy expressions. Using this scheme, terms up to second order (ϵ^2, with $\epsilon \ll 1$) are retained. In addition, some third order terms related to elastic torsion are also retained. The assumed orders of the blade deformations are $u_e = O(\epsilon^2)$, v_b and $w_b = O(\epsilon)$, $\hat{\phi} = O(\epsilon)$, and v_s and $w_s = O(\epsilon^2)$. This ordering scheme is appropriate for the hingeless blades examined in this study. However, bearingless rotor flexbeams can experience large torsional deformations and may require modifications to the assumed order of the total elastic twist $\hat{\phi}$. The resulting variational form of strain energy is given in Appendix A of Ref. 45 and in Ref. 46. Assumed orders for all remaining variables are also included in Ref. 46. In general, the strain energy is a function of the elastic constants of the blade as shown symbolically by

$$\delta U = \delta U_I + \delta U_C$$

$$\delta U_I = \delta U_I(EA, GJ, EI_y, EI_z, GA_y, GA_z, EC_1, EC_2, EB_1, EB_2)$$

$$\delta U_C = \delta U_C(K_{12}, K_{13}, K_{14}, K_{25}, K_{36}, K_{45}, K_{46}) \tag{7}$$

where δU_I represents the strain energy components for an isotropic blade, and δU_C represents the additional strain energy components due to composite elastic coupling effects. The nature of these coupling is also discussed in Refs. 24, 45, and 46. Additional coupling terms will also exist for blade spars with no geometric or material symmetry. Provided that no dramatic geometric or material asymmetry exists, the present formulation can be used to access the aeroelastic behavior of general composite cross-section blades if a preprocessor analysis is used to evaluate the beam stiffness coefficients. It should also be noted that the present formulation is most applicable to helicopter blades with small or moderate amounts of pretwist. Modifications for highly pretwisted blades would focus on employing more detailed representations of section warping and centrifugal torsional stiffening effects.

The kinetic energy δT and virtual work δW are also formulated for use in Hamilton's principle. The kinetic energy is not a function of the elastic constants of the beam; therefore, the kinetic energy is identical for both isotropic and composite blades. The variational form of the kinetic energy (including shear deformation) is also given in Refs. 45 and 46. In the present formulation, the effects of centrifugal and Coriolis forces are captured in the kinetic energy expression. External aerodynamic forces on the rotor blade contribute to the virtual

work variational δW. Aerodynamic forces and moments are calculated using both quasisteady and unsteady strip theory. The effects of compressibility and reversed flow are also included in the aerodynamic models. Drees linear inflow model is used for the rotor inflow distribution.

Spatial Finite Element Discretization

The variational form of Hamilton's principle is discretized using shear flexible beam finite elements. This discretization is shown by

$$\delta\Pi = \int_{t_1}^{t_2} (\delta U - \delta T - \delta W)\, dt = 0 \tag{8}$$

$$\delta\Pi = \int_{\psi_1}^{\psi_F} \sum_{i=1}^{N} (\delta U_i - \delta T_i - \delta W_i)\, d\psi = 0 \tag{9}$$

with δU_i, δT_i, and δW_i defined as the elemental contributions to the strain energy variation, kinetic energy variation, and virtual work, and N as the total number of beam finite elements. Each beam element consists of 19 degrees of freedom (DOF) (see Fig. 1). Four additional degrees of freedom (compared to existing rotor blade finite elements as in Ref. 47) are introduced to accurately model the effects of transverse shear-related deformations and couplings. These degrees of freedom correspond to cubic variations in axial elastic and (flap and lag) bending deflections, quadratic variation in elastic torsion, and linear variation in (flap and lag) transverse shear deformations. Some general characteristics of this type of shear flexible beam element are discussed in Ref. 48 for nonrotating isotropic beams.

Coupled Trim Solution and Shaft-Fixed Aeroelastic Stability

For the aeroelastic response and loads analysis, the new structural formulation just described for the composite blade is integrated with the comprehensive aeroelastic analysis UMARC (University of Maryland Advanced Rotorcraft Code).[49] The finite element equations are transformed to normal mode space to facilitate an efficient solution for the blade response. The nonlinear, periodic normal mode equations are then solved for steady response using a time finite element technique. Steady and vibratory components of the rotating frame blade loads (i.e., shear forces and bending/torsion moments) are calculated using the force summation method. In this approach, blade aerodynamic and inertia forces are directly integrated over the desired length of the blade. Fixed frame hub loads are calculated by summing the contributions from individual blades. A coupled trim procedure is carried out to solve for the blade response, pilot control inputs, and vehicle orientation simultaneously. The coupled trim procedure is essential for composite rotors because the elastic blade deflections play a significant role in the net forces and moments generated by the rotor. After the coupled trim response is computed, blade natural frequencies and mode shapes are recalculated about the (time averaged) deflected position. The linearized blade equations are numerically transformed from the rotating frame to the fixed frame using the Fourier coordinate transformation (FCT). Quasisteady aerodynamics are used for all stability calculations. Low frequency unsteady aerodynamic effects are modeled using a three state dynamic inflow model. After the FCT, the fixed-frame blade equations are augmented by the dynamic inflow equations. The forward flight aeroelastic stability analysis is then performed using Floquet theory. Additional details on the UMARC analysis can be found in Ref. 49.

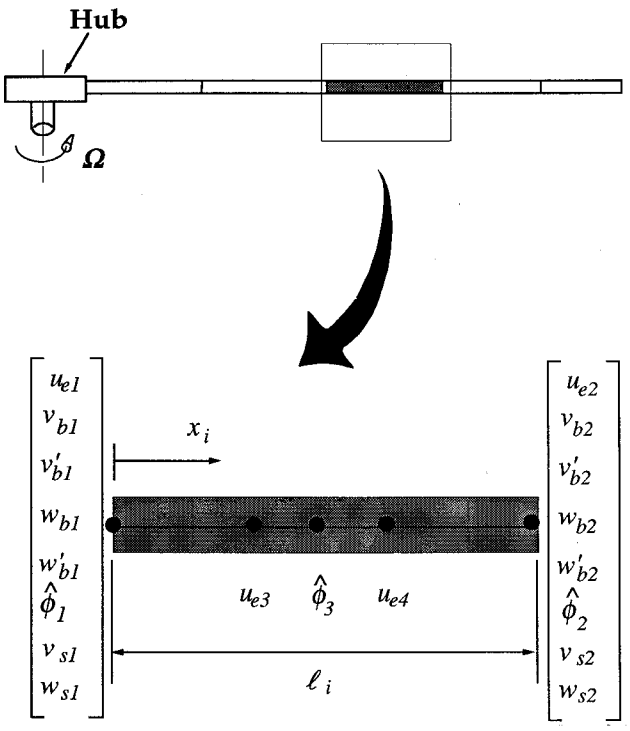

Fig. 1 Nineteen degree-of-freedom shear flexible beam element used for rotor blade.

Results and Discussion

Composite Box-Beam Vibration Correlation

The structural dynamic analysis for the rotating composite beams is evaluated by correlating with both experimental data and detailed finite element results. Elastic properties for the graphite/epoxy (AS4-3501-6) test beams are given in Refs. 34 and 49 as $E_L = 20.59$ msi, $E_T = 1.42$ msi, $G_{LT} = 0.89$ msi, and $\nu_{LT} = 0.42$ msi. The test beams are 33.25 in. long with outer box dimensions of 0.953 and 0.537 in.. Each box-beam wall consists of six graphite/epoxy plies ($t_{\text{ply}} = 0.005$ in.), and the mass density is 0.0001352 lb-s^2/in.^{4}. The experimental data are taken from Ref. 34. Graphite/epoxy box-beams were fabricated and dynamically tested under both nonrotating and rotating (up to approximately 1000 rpm) conditions in a vacuum chamber test facility. Natural frequencies and mode shapes were measured for the first two flap bending modes and the first lag bending mode. Detailed finite element results are calculated using the analysis developed by Stemple and Lee.[12] This formulation uses a shear flexible beam element with warping displacements parallel to the deformed beam axis. The fully coupled warping displacements are then superimposed over the cross section. Natural vibration mode shapes and frequencies are calculated using a subspace iteration technique. For this comparison, five natural modes are examined (two flap, two lag, and one torsion). Calculations were performed using five spanwise elements and four cross-sectional warping elements in each spanwise element. Results from the present analysis (designated UMARC 19 DOF) were calculated using eight shear flexible spanwise elements. It should be noted that elastic coupling results in coupled beam mode shapes. For example, the "flap" mode for a beam with bending-torsion coupling is more accurately defined as a combined "flap-torsion" mode.[33-35,47]

The comparison is conducted for six different box-beam configurations. Three configurations are antisymmetric layup beams featuring extension-torsion and bending-shear couplings. Layup details for these six test beams are given in Ref. 49. Comparative results are presented in Tables 1a and 1b. The correlation between the three sets of results is generally very good (on the order of 5-10% differences). Margins of error between the detailed finite element results and the UMARC results are a result of the simplified cross-section analysis for the composite stiffness coefficients. Similar margins of error were also observed in a static deflection correlation study in Ref. 24. Note the influence of the transverse shear couplings shown in Table 1b. Neglecting bending-shear couplings K_{25} and K_{36} causes errors on the order of 20% in flap

Table 1a Rotating frequencies (Hz) of symmetric layup box-beams

	$(15)_6$, $(15/-15)_3$ at $\Omega=1002$ rpm			$(30)_6$, $(30/-30)_3$ at $\Omega=1014$ rpm			$(45)_6$, $(45/-45)_3$ at $\Omega=1008$ rpm		
Mode	Experiment	Detailed FEM[a]	UMARC (19 DOF)	Experiment	Detailed FEM	UMARC (19 DOF)	Experiment	Detailed FEM	UMARC (19 DOF)
Flap 1	35.20	36.00	36.87	28.60	27.33	18.13	25.63	23.48	23.91
Flap 2	188.0	197.3	203.0	135.0	133.6	139.8	118.3	102.1	105.8
Lag 1	53.80	57.10	62.45	39.50	38.66	42.85	33.00	26.30	27.79
Lag 2	NA	349.3	378.9	NA	236.3	261.3	NA	162.8	171.5
Torsion 1	NA	714.9	729.2	NA	872.9	936.1			

[a]FEM = finite element method.

Table 1b Rotating frequencies (Hz) of antisymmetric layup box-beams

	$(15)_6$ at $\Omega=1002$ rpm				$(0/30)_3$ at $\Omega=1002$ rpm				$(0/45)_3$ at $\Omega=1002$ rpm			
Mode	Experiment	Detailed FEM[a]	UMARC (19 DOF)	UMARC (no shear)	Experiment	Detailed FEM	UMARC (19 DOF)	UMARC (no shear)	Experiment	Detailed FEM	UMARC (19 DOF)	UMARC (no shear)
Flap 1	33.60	34.63	36.49	43.52	36.40	38.71	39.54	40.93	35.90	37.17	37.57	37.77
Flap 2	184.0	188.0	202.2	247.8	209.0	215.8	222.3	231.4	191.0	205.0	209.0	210.0
Lag 1	46.6	47.31	53.73	62.57	50.60	54.38	56.42	58.20	50.0	51.60	52.44	52.71
Lag 2	NA	287.2	328.2	383.6	NA	334.6	348.2	348.2	NA	317.6	324.6	326.18
Torsion 1	NA	513.2	493.7	493.7	NA	676.3	665.0	664.0	NA	658.7	647.7	647.7

[a]FEM = finite element method.

Table 2 Vehicle and rotor properties (nominal condition)

Main rotor	
Number of blades	4
Radius, ft	16.2
Hover tip speed, ft/s	650
Airfoil	NACA 0015
c_0, c_1	0.0, 5.73
d_0, d_1, d_2	0.0095, 0.0, 0.2
c/R	0.08
t/R	0.15
Solidity, σ	0.10
C_T/σ	0.07
Precone, β_p	0.0
Lock number, γ	6.34
Mass per unit length, slug/ft	0.135
Torsional inertias, km_1^2/R^2, km_2^2/R^2	0.0001, 0.0004
Hub length, x_{hub}/R	0.04
Aerodynamic root cutout, x_{root}/R	0.10
Tail rotor and horizontal tail	
Tail rotor radius, ft	3.24
Tail rotor solidity, σ_{tr}	0.15
Tail rotor gear ratio, Ω_{tr}/Ω_{mr}	5.0
Tail rotor location, x_{tr}/R	1.2
Tail rotor above c.g., h_{tr}/R	0.2
$(c_0)_{tr}$, $(c_1)_{tr}$	0.0, 6.0
Horizontal tail location, x_{ht}/R	0.95
Horizontal tail planform area, $S_{ht}/\Pi R^2$	0.011
$(c_0)_{ht}$, $(c_1)_{ht}$	0.0, 6.0
Vehicle	
Total vehicle weight, lb	5800
Longitude and latitude offsets, $x_{c.g.}/R$, $y_{c.g.}/R$	0.0, 0.0
c.g. below hub, h/R	0.2
Flat plate area, f/PR^2	0.01

Table 3 Composite blade spar laminates

Baseline	Wall laminates
Top	$[0_3/(15/-15)_3/(45/-45)_2]_s$
Bottom	$[0_3/(15/-15)_3/(45/-45)_2]_s$
Right	$[0_3/(15/-15)_3/(45/-45)_2]_s$
Left	$[0_3/(15/-15)_3/(45/-45)_2]_s$
Symmetric A	Wall laminates
Top	$[0_3/(-15)_6/(45/-45)_2]_s$
Bottom	$[0_3/(-15)_6/(45/-45)_2]_s$
Right	$[0_3/(15/-15)_3/(45/-45)_2]_s$
Left	$[0_3/(15/-15)_3/(45/-45)_2]_s$
Symmetric B	Wall laminates
Top	$[0_3/(15)_6/(45/-45)_2]_s$
Bottom	$[0_3/(15)_6/(45/-45)_2]_s$
Right	$[0_3/(15/-15)_3/(45/-45)_2]_s$
Left	$[0_3/(15/-15)_3/(45/-45)_2]_s$
Symmetric C	Wall laminates
Top	$[0_3/(15/-15)_3/(45/-45)_2]_s$
Bottom	$[0_3/(15/-15)_3/(45/-45)_2]_s$
Right	$[0_3/(15)_6/(45)_6]_s$
Left	$[0_3/(15)_6/(45)_6]_s$
Antisymmetric	Wall laminates
Top	$[0_3/(-15)_6/(45/-45)_2]_s$
Bottom	$[0_3/(15)_6/(45/-45)_2]_s$
Right	$[0_3/(15)_6/(45/-45)_2]_s$
Left	$[0_3/(-15)_6/(45/-45)_2]_s$

and lag frequencies of the $(15)_6$ antisymmetric layup beam. These couplings play a much smaller role for the $(0/30)_3$ and the $(0/45)_3$ antisymmetric layup beams (see Table 1b). These trends are consistent with the results of the static deflection investigation presented in Ref. 24.

Soft-In-plane Hingeless Rotor Helicopter in Free Flight Propulsive Trim Condition

Using the newly developed comprehensive aeroelastic analysis for composite rotor blades, the aeroelastic response and loads of a helicopter with elastically coupled rotor blades is investigated. Both the vehicle and rotor configurations (including spar dimension and ply orientations) have been carefully selected to be as representative of an actual system as possible. The properties of the vehicle for the test cases are given in Table 2. The vehicle properties are similar to the BO-105 hingeless rotor design. The most notable differences are the increased chord size (and solidity), slightly increased Lock number, and different airfoil section. The rotor spar is designed to yield realistic magnitudes of cross-section stiffness, inertia, and rotating natural frequencies. Because of the very high specific stiffness of the graphite/epoxy spar material, nonstructural mass is required to bring the rotor mass and torsion inertia up to realistic levels. Unrealistically low torsion inertia was observed to result in a flutter-type instability in forward flight. Spar material properties are identical to those provided in Ref. 46. The outer box spar width is 4.2 in., the outer spar depth is 2.2 in., and each of the four spar walls contains 26 graphite/epoxy plies. In the present study, five different composite laminate designs are evaluated. The laminates used in

the spar walls are given in Table 3. Ply orientation angles are defined as positive toward the leading edge for the horizontal spar walls (top and bottom) and positive toward the top of the blade section for the vertical spar walls. In Table 3, "right" refers to the spar wall nearest to the trailing edge of the airfoil. The baseline case exhibits no elastic couplings. Symmetric cases A and B exhibit pitch-flap and extension-lag shear couplings. In terms of the designations defined in Ref. 50, symmetric case A exhibits negative pitch-flap coupling (pitch increases when blade flaps up, $\delta_3 < 0$, $K_{45} < 0$), and symmetric case B exhibits positive pitch-flap coupling. In terms of the designations defined in Ref. 50, symmetric case C exhibits negative pitch-lag coupling (pitch increases when blade lags back, $\delta_4 > 0$, $K_{45} > 0$) and extension-flap shear coupling. The antisymmetric case exhibits extension-torsion (nose-down elastic twist due to tension) and bending-shear couplings. A schematic view of the blade spar and the lamination details for symmetric case A are shown in Fig. 2. For the uniform blades considered in the present investigation, five spatial elements are used. Forward flight steady response is computed using six fourth-order-time finite elements and the modal basis consists of eight normal modes.

The selection of the test cases was designed to minimize the variations of direct stiffness changes and natural frequency placement on the comparisons between the baseline and coupled blades. This is helpful for evaluation of elastic coupling effects because differences between elastically coupled blades and the baseline blade cannot be attributed to variations in these important parameters. Elastic stiffnesses (including coupling stiffnesses) for all of the test cases are provided in Ref. 46. Rotating natural frequencies for all the test cases are also provided in Ref. 46. The baseline blade had nondimensional (ω/Ω) fundamental rotating flap, lag, and torsion frequencies of 1.15, 0.75, and 4.59, respectively. Despite the presence of the elastic couplings, there was very little difference (<2%) between the natural frequencies of the coupled blades and baseline uncoupled blade. The mode shapes, however, are significantly altered by the elastic couplings. The coupling of the deflection modes (e.g., flap-torsion, lag-torsion, and extension-torsion) manifests directly in the static and dynamic blade response. As shown in Ref. 46, elastic pitch-flap couplings (symmetric A, B) resulted in approximately 2 deg of static elastic twist in hover whereas extension-torsion coupling (antisymmetric) results in approximately 5 deg of static elastic twist in hover. The baseline blade is essentially untwisted in hover (elastic twist < 0.5 deg). The symmetric C case (pitch-lag elastic coupling) is also essentially untwisted in hover (elastic twist

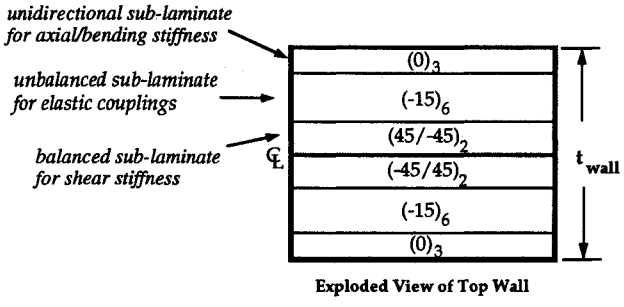

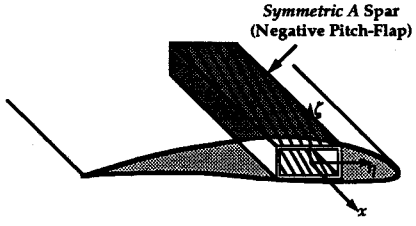

Fig. 2 Schematic of symmetric A layup blade spar.

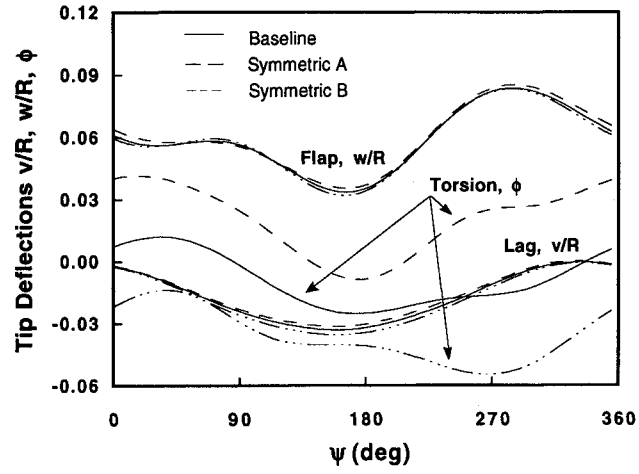

Fig. 3 Baseline, symmetric A, and symmetric B tip deflections in forward flight ($\mu = 0.35$, $C_T/\sigma = 0.07$).

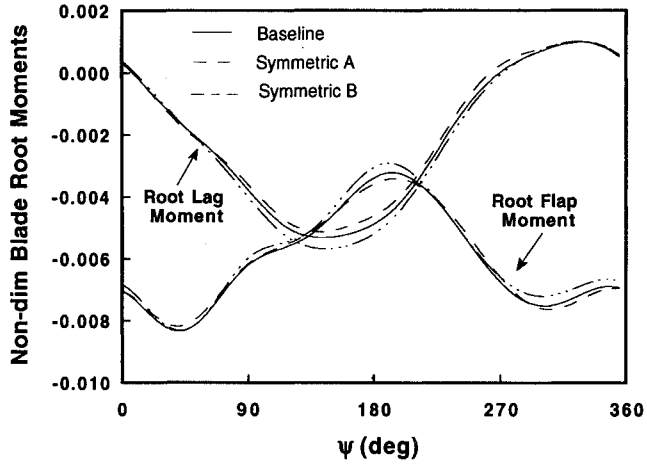

Fig. 4 Baseline, symmetric A, and symmetric B root bending moments in forward flight ($\mu = 0.35$, $C_T/\sigma = 0.07$).

< 0.2 deg). The symmetric C case is significantly coupled; however, the applied lag forces and resulting lag deflections are very low in the hover condition. This result is in contrast to the applied flap forces (lift) and axial forces (centrifugal), which result in higher levels of elastic twist. It is important to note that only very light amounts of elastic coupling (indicated by the negligible change in natural frequencies) can generate significant effects in the rotor system behavior. The following discussions elaborate on this observation.

Symmetric Cases A and B (Pitch-Flap Couplings)

Flap, lag, and torsion tip deflections are shown in Fig. 3 for an advance ratio $\mu = V/\Omega R = 0.35$. Both the magnitude and the phase of the torsion response is significantly changed (relative to the baseline blade) due to the elastic couplings. However, the flap response is unchanged, and the lag response is altered only slightly. Throughout this study, blade root shear forces and moments are presented in nondimensional form as

$$\text{nondimensional force} = \frac{F}{m_0 \Omega^2 R^2} \tag{10a}$$

$$\text{nondimensional moment} = \frac{M}{m_0 \Omega^2 R^3} \tag{10b}$$

Magnitudes of the 4-revolution vibratory hub shears and moments are nondimensionalized with respect to the magnitudes of the zero harmonic (constant) vertical hub shear and zero

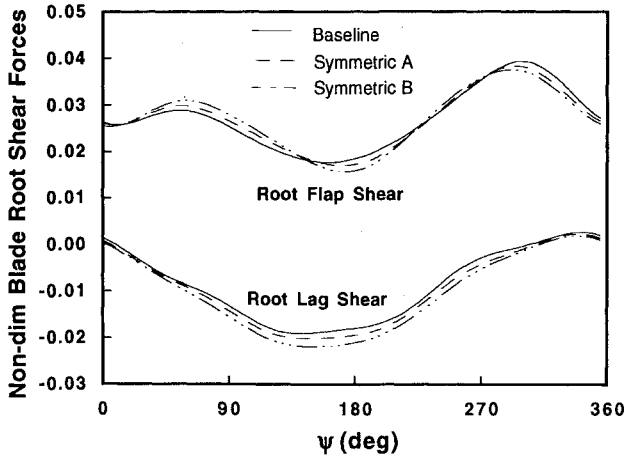

Fig. 5 Baseline, symmetric A, and symmetric B root shear forces in forward flight ($\mu = 0.35$, $C_T/\sigma = 0.07$).

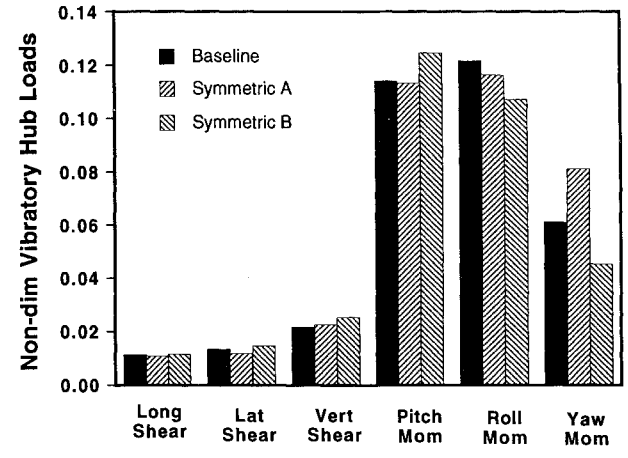

Fig. 6 Baseline, symmetric A, and symmetric B 4-revolution hub loads in forward flight ($\mu = 0.35$, $C_T/\sigma = 0.07$).

harmonic (constant) yaw moment, respectively. For the (uniform) test cases, m_0 reduces to the section mass per unit length. For an advance ratio of $\mu = 0.35$, the nondimensional blade root bending moments and shear forces are shown in Figs. 4 and 5. These results indicate that the elastic couplings have only a small effect on the blade root loads.

For these cases, the most notable effect is the collective pitch change due to varying amounts of steady elastic twist. Cyclic pitch controls are only slightly changed by the elastic couplings. The 4-revolution components of the fixed-frame hub loads are shown in Fig. 6 ($\mu = 0.35$). Elastic couplings have a measurable effect on the vibratory hub moments. This phenomenon is primarily due to the change in phasing of the blade torsion response. Figure 7 shows the variation of regressive (low frequency cyclic) lag mode damping with forward speed. The stability margins of the symmetric B blade are decreased. Symmetric case A is stabilizing in hover; however, as the forward speed increases, this blade becomes less stable than the baseline case. This degradation of blade stability in forward flight was not observed in the earlier composite rotor stability analysis of Ref. 3.

Symmetric Case C (Pitch-Lag Coupling)

Flap, lag, and torsion tip deflections are shown in Fig. 8 for an advance ratio $\mu = 0.35$. The torsion response is again significantly changed due to the elastic coupling. For this case, both the flap response and the lag response are unchanged compared to the baseline blade. For an advance ratio of $\mu = 0.35$, the nondimensional blade root bending moments are also shown in Ref. 46. These results indicate that the elastic couplings have a negligible effect on the blade root loads. The 4-revolution vibratory components of the fixed-frame hub loads are shown in Fig. 9 ($\mu = 0.35$). Elastic couplings cause only a small increase in the vibratory hub moments. This result is once again primarily due to the change in phasing of the blade torsion response. Variation in the regressive lag mode damping with forward speed is shown in Fig. 10. The symmetric C (negative pitch-lag coupling) blade is significantly more stable than the baseline blade throughout the entire range of vehicle forward speeds. In Ref. 46, the symmetric C blade also

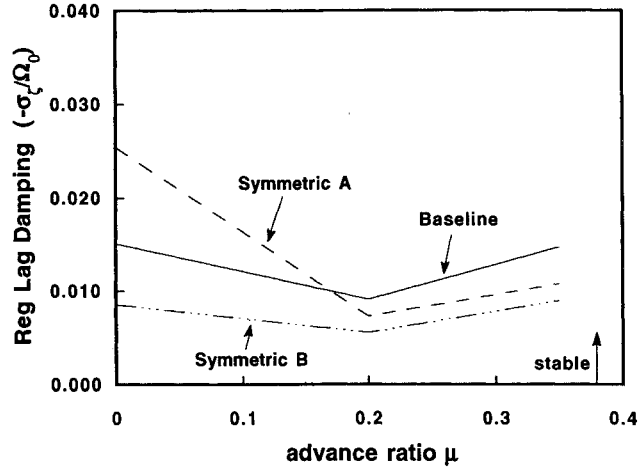

Fig. 7 Variation in baseline, symmetric A, and symmetric B regressive lag mode decay rates with advance ratio ($C_T/\sigma = 0.07$).

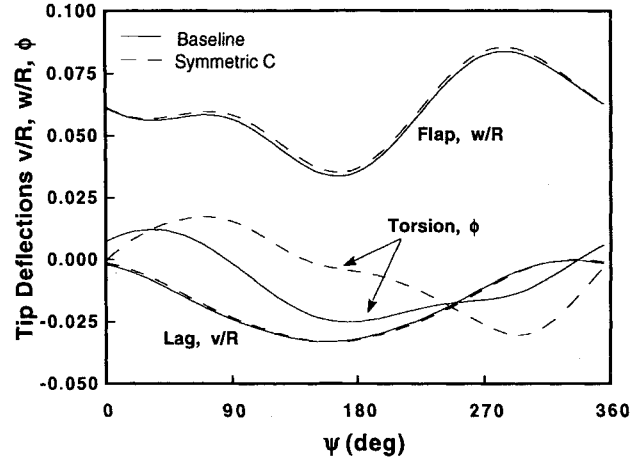

Fig. 8 Baseline and symmetric C tip deflections in forward flight ($\mu = 0.35$, $C_T/\sigma = 0.07$).

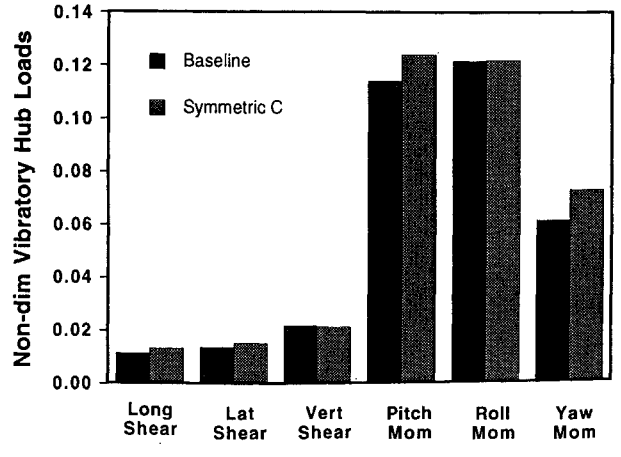

Fig. 9 Baseline and symmetric C vibratory 4-revolution hub loads in forward flight ($\mu = 0.35$, $C_T/\sigma = 0.07$).

demonstrated significant improvements in lag mode damping for both low thrust and high thrust conditions (up to $C_T/\sigma = 0.16$) in hover. The results shown in Fig. 10 and Ref. 46 demonstrate the effectiveness of elastic tailoring to improve aeroelastic stability over a wide range of operating conditions. It should be noted that the overall stabilizing trends of elastic pitch-lag coupling are consistent with the results predicted in Ref. 3.

Antisymmetric Case (Extension-Torsion Coupling)

As mentioned earlier, the antisymmetric layup blade undergoes approximately 5 deg of nose-down elastic twist due to axial centrifugal forces and extension-torsion elastic coupling. This magnitude of static twist significantly shifts the blade lift distribution inboard and results in a direct reduction of flap response and corresponding reduction in blade loads. Because of this effect, it is necessary to judge the unique behavior of the antisymmetric layup blade against a pretwisted baseline blade. Tip deflections for the antisymmetric and pretwisted baseline blades are shown in Fig. 11 for an advance ratio of $\mu = 0.35$.

Flap and lag deflections of the antisymmetric blade are very similar to the baseline pretwisted blade. As discussed, the elastic twist angle is dramatically changed due to elastic extension-torsion coupling. The trim flight controls are shown in Ref. 46. In addition to the collective pitch angle, a measurable increase in tail rotor pitch is observed for the coupled blade. This is directly linked to an increase in steady rotor torque. For an advance ratio of $\mu = 0.35$, the nondimensional blade root bending moments are also shown in Ref. 46. The lag bending moment is slightly reduced for the antisymmetric blade, and

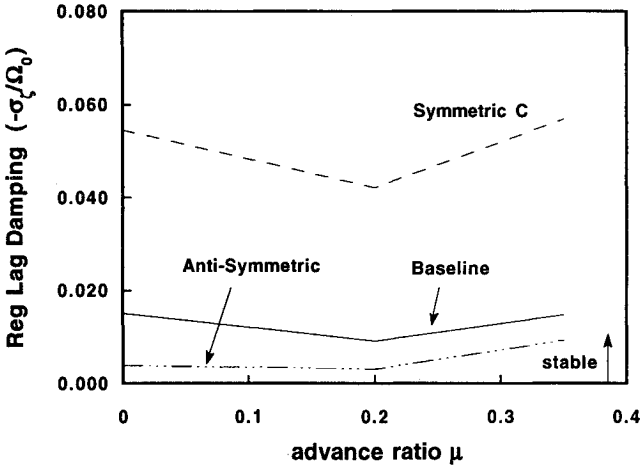

Fig. 10 Variation in baseline, symmetric C, and antisymmetric regressive lag mode decay rates with advance ratio ($C_T/\sigma = 0.07$).

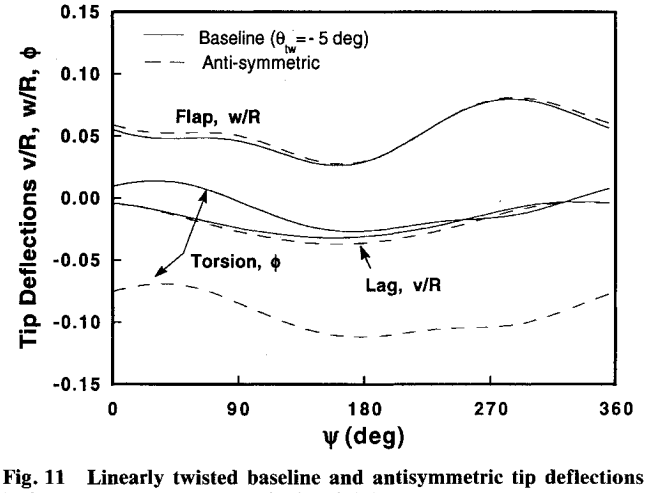

Fig. 11 Linearly twisted baseline and antisymmetric tip deflections in forward flight ($\mu = 0.35$, $C_T/\sigma = 0.07$).

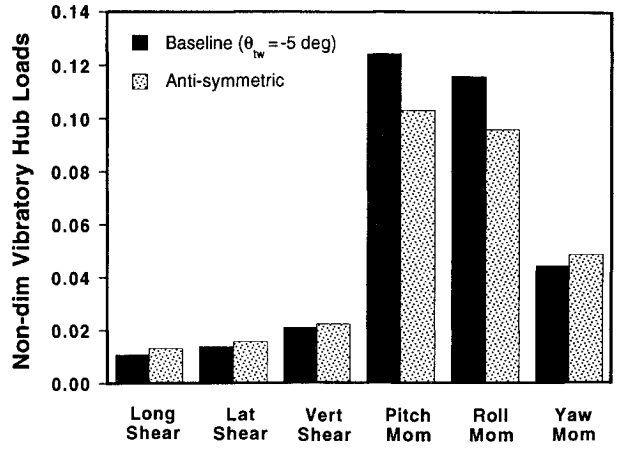

Fig. 12 Linearly twisted baseline and antisymmetric vibratory 4-revolution hub loads in forward flight ($\mu = 0.35$, $C_T/\sigma = 0.07$).

the flap moment is unchanged. The 4-revolution vibratory hub loads are shown in Fig. 12. Notable reductions in vibratory pitch and roll hub moments are observed for the coupled blade. The variation of regressive lag mode damping with forward speed is shown in Fig. 10. These results indicate that the stability margin of the antisymmetric blade is decreased over the entire range of flight speeds. This behavior is also consistent with the blade stability results presented in Ref. 3.

Unsteady Aerodynamics Results

All of the preceding results are based on quasisteady aerodynamic theory. The effects of linear attached flow unsteady aerodynamics are addressed in detail in Ref. 6. For the sake of brevity, only the important conclusions are summarized in this paper. Unsteady aerodynamic effects significantly influence the magnitude and phase of the flap response. For the baseline case, only small changes in the lag and torsion responses are observed. Elastic coupling between pitch and flap causes the unsteady aerodynamics to influence the torsion response of the symmetric A blade (negative pitch-flap coupling) as well. Very small changes in root moments are observed due to the unsteady effects. The change in vibratory hub loads is, however, more significant. For the baseline and symmetric A blades, unsteady effects cause a significant increase in the 4-revolution vibratory shear forces and moments. This increase is primarily a result of the changes in phase and magnitude of the flap response. Comparing the elastically coupled blade to the baseline blade (both unsteady results), the coupled blade results in small increases in vibration. This is the same trend established using the quasisteady aerodynamic model (see Fig. 6). Similar effects of unsteady aerodynamics are also observed for the symmetric C blade (negative pitch-lag coupling).

Conclusions

A comprehensive finite element based aeroelastic analysis for elastically tailored composite helicopter rotor blades has been developed. The new structural model in this analysis includes the effects of transverse shear, an improved model of torsion-related out-of-plane warping, and two-dimensional in-plane elasticity. A new 19 degree-of-freedom transverse-shear flexible beam element is integrated with the University of Maryland Advanced Rotorcraft Code. Fully coupled aeroelastic trim and shaft-fixed aeroelastic stability have been calculated using the new analysis. The structural dynamic analysis has been evaluated for rotating composite beams by correlating with both experimental data and detailed finite element results. Correlation of natural frequencies for both symmetric and antisymmetric layup graphite/epoxy box-beams was generally very good. The margins of error (5–10%) were as a result of simplifying assumptions in the cross-sectional analysis.[24]

The following conclusions are based on the application of the aeroelastic analysis to a soft-in-plane hingeless rotor helicopter:

1) The selection of suitable test cases successfully negated the effects of direct stiffness and frequency placement changes on the evaluation of elastic coupling effects.

2) Forward flight aeroelastic response calculations indicated that the magnitude and phase of torsion response is significantly affected by elastic couplings. Variations in flap and lag responses are generally small.

3) Blade root bending moments and shear forces were not dramatically altered by the elastic couplings. In some cases, vibratory hub loads were measurably changed as a result of the elastic couplings. For example, the antisymmetric blades reduced vibratory 4-revolution pitch and roll moments by approximately 15% relative to a comparably twisted baseline blade.

4) The shaft-fixed aeroelastic stability (lag mode damping) was significantly affected by the elastic couplings. The symmetric layup blade with negative pitch-lag coupling (symmetric C) demonstrated more than 300% increases in lag mode damping. This stabilizing mechanism was effective over a range of thrust levels and advance ratios ($\mu = 0.0$ to 0.35). The damping of the positive pitch-flap (symmetric B) and extension-torsion (antisymmetric) coupled blades was decreased over the range of advance ratios $\mu = 0.0$ to 0.35. The blades with negative elastic pitch-flap coupling (symmetric A) showed increased stability in hover; however, as the forward speed increased, the lag damping dropped below the baseline blade damping.

5) Unsteady aerodynamic effects resulted in a magnitude and phase change of the blade flap response. Smaller changes were observed for lag and torsion responses. The change in response manifested as a substantial increase in vibratory 4-revolution hub loads. Trends in the effects of elastic coupling on the response and loads were similar using both quasisteady and unsteady aerodynamics.

Acknowledgments

This research was jointly supported by the Army Aerostructures Directorate, Grant NAG-1-1253, technical monitor William T. Yeager, Jr. and the Army Research Office, Contract DAAL-03-88-C0002, and technical monitors Robert Singleton and Tom Doligalski. The authors would like to thank Alan Stemple of McDonnell Douglas Helicopter Corporation for help in making his finite element program available.

References

[1]Hong, C.-H., and Chopra, I., "Aeroelastic Stability Analysis of a Composite Rotor Blade," *Journal of the American Helicopter Society,* Vol. 30, No. 2, 1985, pp. 57–67.

[2]Hong, C.-H., and Chopra, I., "Aeroelastic Stability Analysis of a Composite Bearingless Rotor Blade," *Journal of the American Helicopter Society,* Vol. 31, No. 4, 1985, pp. 29–35.

[3]Panda, B., and Chopra, I., "Dynamics of Composite Rotor Blades in Forward Flight," *Vertica,* Vol. 11, No. 1/2, 1987, pp. 107–209.

[4]Nixon, M. W., "Extension-Twist Coupling of Composite Circular Tubes With Application to Tilt Rotor Blade Design," *Proceedings of the AIAA/ASME/ASCE/AHS 28th Structures, Structural Dynamics and Materials Conference* (Monterey, CA), AIAA, Washington, DC, 1987, pp. 295–303 (AIAA Paper 87-0772).

[5]Worndle, R., "Calculation of The Cross Section Properties and The Shear Stress of Composite Rotor Blades," *Vertica,* Vol. 6, No. 2, 1982, pp. 111–129.

[6]Giavotto, V., Borri, M., et al., "Anisotropic Beam Theory and Applications," *Computers and Structures,* Vol. 16, No. 1–4, 1983, pp. 403–413.

[7]Borri, M., and Merlini, T., "A Large Displacement Formulation For Anisotropic Beam Analysis," *Mechanica,* Vol. 21, 1986, pp. 30–37.

[8]Bauchau, O. A., and Hong, C.-H., "Finite Element Approach to Rotor Blade Modeling," *Journal of the American Helicopter Society,* Vol. 32, No. 1, 1987, pp. 60–67.

[9]Bauchau, O. A., and Hong, C.-H., "Large Displacement Analysis of Naturally Curved and Twisted Composite Beams," *AIAA Journal,* Vol. 25, No. 10, 1987, pp. 1469–1475.

[10]Bauchau, O. A., and Hong, C.-H., "Nonlinear Composite Beam Theory," *Journal of Applied Mechanics,* Vol. 55, No. 1, March 1988, pp. 156–163.

[11]Stemple, A. D., and Lee, S. W., "Finite Element Model For Composite Beams With Arbitrary Cross Sectional Warping," *AIAA Journal,* Vol. 26, No. 12, 1988, pp. 1512–1520.

[12]Stemple, A. D., and Lee, S. W., "Large Deflection Static and Dynamic Finite Element Analysis of Composite Beams with Arbitrary Cross Sectional Warping," *Proceedings of the AIAA/ASME/ASCE/AHS/ASC 30th Structures, Structural Dynamics and Materials Conference* (Mobile, AL), AIAA, Washington, DC, 1989, pp. 1788–1798 (AIAA Paper 89-1363).

[13]Kosmatka, J. B., "A Refined Beam Theory For Advanced Composite Rotor Blade Analysis," *Proceedings of the American Helicopter Society National Technical Specialists' Meeting on Advanced Rotorcraft Structures* (Williamsburg, VA), Oct. 1988.

[14]Kosmatka, J. B., "Extension, Bending and Torsion of Anisotropic Beams With Initial Twist," *Proceedings of the AIAA/ASME/ASCE/AHS/ASC 30th Structures, Structural Dynamics and Materials Conference* (Mobile, AL), AIAA, Washington, DC, 1989, pp. 1799–1806 (AIAA Paper 89-1364).

[15]Kosmatka, J. B., and Friedmann, P. P., "Vibration Analysis of Composite Turbo-Propellers Using a Nonlinear Beam-Type Finite Element Approach," *AIAA Journal,* Vol. 27, No. 11, 1989, pp. 1606–1614.

[16]Mansfield, E. H., and Sobey, A. J., "The Fibre Composite Helicopter Blade; Part 1: Stiffness Properties; Part 2: Prospects for Aeroelastic Tailoring," *Aeronautical Quarterly,* Vol. 30, No. 2, May 1979, pp. 413–449.

[17]Rehfield, L. W., "Design Analysis Methodology for Composite Rotor Blades," *Seventh DoD/NASA Conference on Fibrous Composites in Structural Design,* AFWAL-TR-85-3094, Denver, CO, June 1985, pp. (v(a)1)–(v(a)15).

[18]Rehfield, L. W., Atilgan, A. R., and Hodges, D. H., "Non-Classical Behavior of Thin-Walled Composite Beams with Closed Cross Sections," *Journal of the American Helicopter Society,* Vol. 35, No. 2, 1990, pp. 42–50.

[19]Bauchau, O. A., "A Beam Theory For Anisotropic Materials," *Journal of Applied Mechanics,* Vol. 52, No. 2, June 1985, pp. 416–422.

[20]Libove, C., "Stresses and Rate of Twist in Single-Cell Thin-Walled Beams with Anisotropic Walls," *AIAA Journal,* Vol. 26, No. 10, 1988, pp. 1006–1118.

[21]Bicos, A. S., and Springer, G. S., "Design of a Composite Box-Beam," *Journal of Composite Materials,* Vol. 20, No. 1, Jan. 1986, pp. 86–109.

[22]Klang, E. C., and Kuo, T. M., "Component Level Analysis of Composite Box-Beams," *Proceedings of the AIAA/ASME/ASCE/AHS/ASC 30th Structures, Structural Dynamics and Materials Conference* (Mobile, AL), AIAA, Washington, DC, 1989 (AIAA Paper 89-1360).

[23]Minguet, P., and Dugundji, J., "Experiments and Analysis for Composite Blades Under Large Deflections Part 1—Static Behavior," *AIAA Journal,* Vol. 28, No. 9, 1990, pp. 1573–1579.

[24]Smith, E. C., and Chopra, I., "Formulation and Evaluation of an Analytical Model for Composite Box-Beams," *Journal of the American Helicopter Society,* Vol. 36, No. 3, 1991, pp. 22–35.

[25]Chandra, R., and Chopra, I., "Experimental and Theoretical Analysis of Composite I-Beams with Elastic Couplings," *AIAA Journal,* Vol. 29, No. 12, 1991, pp. 2197–2205.

[26]Abarcar, R. B., and Cunniff, P. F., "The Vibration of Cantilever Beams of Composite Material," *Journal of Composite Materials,* Vol. 6, No. 10, 1972, pp. 504–517.

[27]Teoh, L. S., and Huang, C. C., "The Vibration of Beams of Fibre Reinforced Material," *Journal of Sound and Vibration,* Vol. 51, No. 4, 1977, pp. 467–473.

[28]Teh, K. K., and Huang, C. C., "The Effects of Fibre Orientation on Free Vibrations of Composite Beams," *Journal of Sound and Vibration,* Vol. 69, No. 2, 1980, pp. 327–337.

[29]Jensen, D. W., Crawley, E. F., and Dugundji, J., "Vibration of Cantilevered Graphite/Epoxy Plates with Bending-Torsion Coupling," *Journal of Reinforced Plastics and Composites,* Vol. 1, No. 7, July 1982, pp. 224–269.

[30]Weisshaar, T. A., and Foist, B. L., "Vibration and Flutter of Advanced Composite Lifting Surfaces," *Proceedings of the AIAA/ASME/ASCE 24th Structures, Structural Dynamics and Materials Conference* (Lake Tahoe, NV), AIAA, New York, 1983 (AIAA Paper 83-0961).

[31]Jensen, D. W., and Crawley, E. F., "Frequency Determination Techniques for Cantilevered Plates with Bending-Torsion Coupling," *AIAA Journal,* Vol. 22, No. 3, 1984, pp. 415–420.

[32]Minguet, P., and Dugundji, J., "Experiments and Analysis for Composite Blades Under Large Deflections Part 2—Dynamic Behavior," *AIAA Journal,* Vol. 28, No. 9, 1990, pp. 1580–1588.

[33]Hodges, D. H., Atilgan, A. R., Fulton, M. V., and Rehfield, L. W., "Free Vibration Analysis of Composite Beams," *Journal of the American Helicopter Society,* Vol. 36, No. 3, 1991, pp. 36–47.

[34]Chandra, R., and Chopra, I., "Experimental-Theoretical Investigation of the Vibration Characteristics of Rotating Composite Box-Beams," American Helicopter Society National Technical Specialists' Meeting on Rotorcraft Dynamics (Arlington, TX), Nov. 1989.

[35]Chandra, R., and Chopra, I., "Vibration Characteristics of Composite I-Beams with Elastic Couplings under Rotation," *Proceedings of the 47th American Helicopter Society Annual Forum* (Phoenix, AZ), May 1991, pp. 661–674.

[36]Rand, O., "Periodic Response of Thin-Walled Composite Blades," *Journal of the American Helicopter Society,* Vol. 36, No. 4, 1991, pp. 3–11.

[37]Chopra, I., "Perspectives in Aeromechanical Stability of Helicopter Rotors," *Vertica,* Vol. 14, No. 4, 1990, pp. 457–508.

[38]Friedmann, P. P., "Rotary-Wing Aeroelasticity with Application to VTOL Vehicles," *Proceedings of the AIAA/ASME/ASCE/AHS/ASC 31st Structures, Structural Dynamics and Materials Conference* (Long Beach, CA), AIAA, Washington, DC, 1990, pp. 1624–1670 (AIAA Paper 90-1115).

[39]Hodges, D., "Review of Composite Rotor Blade Modeling," *AIAA Journal,* Vol. 28, No. 3, 1990, pp. 561–564.

[40]Kaza, K. R., and Kvaternik, R. G., "Nonlinear Aeroelastic Equations for Combined Flapwise Bending, Chordwise Bending, Torsion, and Extension of Twisted Nonuniform Rotor Blades in Forward Flight," NASA TM 74059, Aug. 1977.

[41]Beddoes, T. S., "Representation of Airfoil Behavior," *Vertica,* Vol. 7, No. 2, 1983, pp. 183–197.

[42]Leishman, J. G., and Beddoes, T. S., "A Generalized Model for Unsteady Aerodynamic Behavior and Dynamic Stall Using the Indicial Method," *Proceedings of the 42nd Annual National Forum of the American Helicopter Society,* Washington, DC, May 1986.

[43]Leishman, J. G., "Validation of Approximate Indicial Aerodynamic Functions for Two-Dimensional Subsonic Flow," *Journal of Aircraft,* Vol. 25, No. 7, 1988, pp. 914–922.

[44]Torok, M. S., and Chopra, I., "Rotor Loads Prediction Utilizing a Coupled Aeroelastic Analysis with Refined Aerodynamic Modeling," *Journal of the American Helicopter Society,* Vol. 36, No. 1, 1991, pp. 58–67.

[45]Sivaneri, N. T., and Chopra, I., "Finite Element Analysis for Bearingless Rotor Blade Aero-Elasticity," *Journal of the American Helicopter Society,* Vol. 29, No. 2, 1984, pp. 42–51.

[46]Smith, E. C., and Chopra, I., "Aeroelastic Response and Blade Loads of a Composite Rotor in Forward Flight," *Proceedings of the AIAA/ASME/ASCE/AHS/ASC 33rd Structures, Structural Dynamics and Materials Conference* (Dallas, TX), AIAA, Washington, DC, 1992, pp. 1996–2014 (AIAA Paper 92-2466).

[47]Smith, E. C., "Aeroelastic Response and Aeromechanical Stability of Helicopters with Elastically Coupled Composite Rotor Blades," Ph.D. Diss., Univ. of Maryland, College Park, MD, Aug. 1992.

[48]Tessler, A., and Dong, S. B., "On a Hierarchy of Conforming Timoshenko Beam Elements," *Computers and Structures,* Vol. 14, No. 3–4, 1981, pp. 335–344.

[49]Bir, G., Chopra, I., Smith, E. C., et al., *University of Maryland Advanced Rotorcraft Code (UMARC) Theory Manual,* UM-AERO Rept. 92-02, College Park, MD, Aug. 1992.

[50]Johnson, W., *Helicopter Theory,* Princeton Univ. Press, Princeton, NJ, 1980, pp. 238, 239.